Electrodeposition of $Fe_{70}Pd_{30}$ nanowires from a complexed ammonium–sulfosalicylic electrolyte with high stability

V. Haehnel [a,b,*], S. Fähler [a], L. Schultz [a,b], H. Schlörb [a]

[a] IFW Dresden, P.O. Box: 270116, 01171 Dresden, Germany
[b] TU Dresden, Faculty of Mechanical Engineering, 01062 Dresden, Germany

ARTICLE INFO

ABSTRACT

A highly stable plating bath for the electrodeposition of Fe–Pd nanowires into nanoporous alumina templates has been developed. Complexing of both metal ions and exchanging Fe^{2+} by Fe^{3+} avoid chemical reduction of Pd ions and, therefore, undesirable deposition. By using a pulse potential mode and appropriate adjustment of deposition potentials homogeneously filled templates without surface deposits and nanowires close to the desired composition of $Fe_{70}Pd_{30}$ have been achieved. These alloy nanowires represent a key step towards nanoactuators based on magnetic shape memory alloys.

© 2010 Elsevier B.V. All rights reserved.

1. Introduction

Various compositions within the Fe–Pd system exhibit excellent functional properties. Palladium-rich FePd alloys show very good hydrogen absorption kinetics [1]. Alloys around the composition $Fe_{50}Pd_{50}$ can order in the $L1_0$ crystal structure. This results in a high uniaxial magnetocrystalline anisotropy making this material interesting for high density data storage [2]. Around $Fe_{70}Pd_{30}$ a martensitic transformation is observed [3]. Furthermore, in this composition range the magnetic shape memory (MSM) effect had been observed [4]. This allows obtaining a huge strain by applying a magnetic field, which increases up to 3% at low temperatures [5]. The combination of magnetic and martensitic order makes this metallic multiferroic system of particular interest for micro- and nanosystems. In addition to thin films [6] $Fe_{70}Pd_{30}$ nanowires are promising for nanoactuators. Without the need of advanced lithography, nanowires electrodeposited within templates represent the ideal wrought material for true nanosystems. The combination with magnetism will boost the number of actuation mechanisms; e.g. by remote actuation by an external magnetic field. While commonly physical methods are used for the growth of Fe–Pd films [7–9], there are successful reports on the preparation by electrodeposition [10,11].

As an efficient preparation route for metallic nanowires electrodeposition into alumina templates is well known [12–14]. This motivated the electrodeposition Fe–Pd nanowires [15–17] and nanotubes [18]. First experiments used a rather simple electrolyte containing plain Fe^{2+} and Pd^{2+} ions at a low pH value of 3 [17]. Though this allowed a variation of composition in a wide range, no details on electrolyte stability had been given. Furthermore, plating baths containing ammonium citrate complexes of both Fe^{2+} and Pd^{2+} [16,19] or ammonium tartrate for Fe^{2+} and citric acid and ammonia for Pd^{2+} [10,18] had been used. The latter electrolytes are designed for alkaline pH values between 8 and 10, a pH range dissolving the nanoporous alumina templates. Also 5-sulfosalicylic acid is suggested to stabilize the Fe^{2+} or Fe^{2+} ion [1,11,15,20], whereas Fei et al. [15] describe a bath at a more suitable pH of 5; Bryden and Ying [1] use pH 6.

These attempts illustrate the challenging codeposition of Fe and Pd, as Pd is much nobler than Fe. The standard electrode potentials $E°$ of the simple metal ions Pd^{2+} and Fe^{2+} differ by 1.4 V [21]. To allow alloy deposition, the electrode potentials of both metals should be approximated, e.g. by either lowering the concentration of the more noble metal and/or complexing [22]. Complexing for instance Pd^{2+} with ammonia $(Pd(NH_3)_4^{2+})$ can successfully reduce the difference in $E°$ of both metal ions to only 0.4 V [21]. However, although alloy deposition appears to be feasible in principle an effective and stable electrolyte is still missing.

The present study analyses the requirements for a highly stable electrolyte allowing reproducible Fe–Pd nanowire deposition. The goal is homogeneous template filling without any undesirable deposition. Finally, the nanowire composition is adjusted to approximately $Fe_{70}Pd_{30}$ using appropriate deposition potentials in potentiostatic or alternating potential mode.

2. Experimental

The preparation of anodic alumina arrays is carried out by the well known two-step anodization process resulting in hexagonal ordered

* Corresponding author. IFW Dresden, P.O. Box: 270116, 01171 Dresden, Germany.
Tel.: +49 351 4659 290; fax: +49 351 4659 500.
E-mail address: v.haehnel@ifw-dresden.de (V. Haehnel).

nanopores [23]. A detailed description is given in a previous paper [24]. Additionally, to obtain a free standing membrane remaining aluminium and the barrier layer were removed by chemical etching using $CuCl_2$ and H_3PO_4 [25]. The typical pore diameter equals 70 nm, the pore length is between 20 μm and 25 μm. xtbfA 200 nm Au film was sputter-deposited onto the backside of the alumina membrane to provide electrical contact and serves as working electrode for electrodeposition. An aqueous electrolyte based on earlier publications [1,15,20] was used as a starting point. First, $PdCl_2$ was dissolved in concentrated HCl and then dropped into concentrated ammonia. By careful heating and stirring the solution becomes clear and aqueous. Secondly, a solution of $FeSO_4 \cdot 7H_2O$ (0.1 M), sulfosalicylic acid $C_7H_6O_6S \cdot 2H_2O$ (0.2 M), $(NH_4)_2SO_4$ (0.3 M) was added to the Pd solution (0.02 M). The final bath compositions are given in brackets. Finally, the bath was adjusted to pH 5 by H_2SO_4 (electrolyte 1). In subsequent experiments $FeSO_4 \cdot 7H_2O$ was substituted by $Fe_2(SO_4)_3 \cdot 9H_2O$ (electrolyte 2). All deposition experiments were performed at room temperature using a Pt foil as counter electrode and a saturated calomel reference electrode (SCE, 241 mV_{SHE}). Electrodeposition was carried out using an EG&G Potentiostat/Galvanostat Model 263 A. Nanowire morphology was examined at cross-sectional membrane areas by high-resolution scanning electron microscopy (HR-SEM, Leo 1530 Gemini/Zeiss, secondary electron and inlense detector). The integral nanowire composition was measured by energy dispersive X-ray spectroscopy (EDX, extbf20 kV, X-Flash detector, Esprit, Bruker system).

3. Results and discussion

Potentiostatic deposition experiments have been carried out using electrolyte 1 at potentials between $-0.8\ V_{SCE}$ and $-1.2\ V_{SCE}$. The nanowire composition is shown in Fig. 1 in dependence on the applied potential. At low overpotentials the more noble Pd is mainly deposited, most probably diffusion-controlled due to its low concentration. Here, the Fe content might originate from underpotential deposition and/or hydroxide incorporation due to pH increase by advanced hydrogen evolution. Close to $-1.0\ V_{SCE}$ significant Fe deposition sets in increasing the Fe content. At high overpotentials ($\leq -1.2\ V_{SCE}$) Fe deposition becomes diffusion-controlled also resulting in a constant composition around $Fe_{90}Pd_{10}$. The desired ratio of $Fe_{70}Pd_{30}$ is achieved between $-1.0\ V_{SCE}$ and $-1.1\ V_{SCE}$. However, the EDX values exhibit only a rough estimation and do not present the composition of a single nanowire, as the penetration depth is in the range of μm and exceeds the dimension of a single nanowire. Exemplarily a cross-sectional micrograph of a sample deposited at $-1.0\ V_{SCE}$ is shown in Fig. 2a. Only very short, fragment-like wires have been observed. Additionally, spherical deposits are found on top of the sample (inset Fig. 2a). Similar wire morphology,
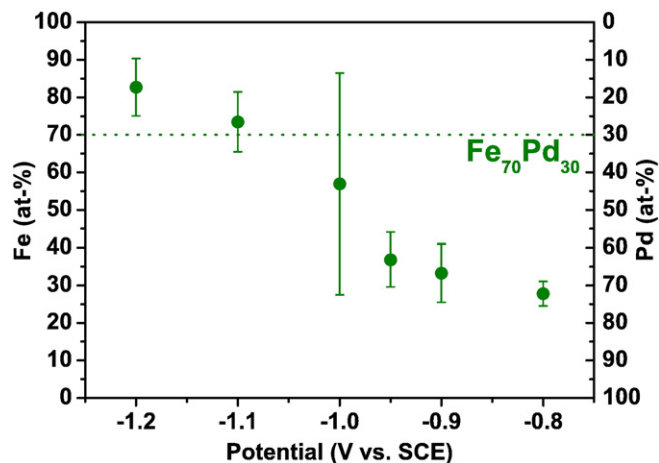
but longer fragments are observed at a more negative potential of $-1.1\ V_{SCE}$. Furthermore, a continuous Fe–Pd layer is formed on top of the membrane. These features can be linked to the measured current vs. deposition time (Fig. 2d). The initial steep increase of the cathodic current (region I) originating from the charging of the electrochemical double layer follows a gradual decrease attributed to the depletion of metal ions at the pore bottom (region II). Simultaneous hydrogen evolution might block pores partially or totally, therefore reducing the deposition area and the measured current and, finally, disrupt the nanowire growth generating an inhomogeneous deposition morphology. The constant current region III is assigned to nanowire growth at stationary conditions. If a pore is completely filled outgrowth takes place. This increases the deposition area and, hence, the deposition current (region IV). This outgrowth leads to large deposits on top that grow together, finally closing other pores from the top. Once a pore is blocked by a gas bubble or at the surface, no further deposition takes place inside.

To overcome the problem of fragmented, short wires and surface coverage an electrodeposition mode using alternating potentials has been applied. This pulse technique decreases concentration gradients, keeps the pH constant and reduces blockingof pores by gas evolution. Pulse plating is also well known to compensate slow diffusion-driven transport in high aspect ratio membranes [14]. During the first step, a potential of $-1.1\ V_{SCE}$ is applied for 60 s. In the second step, a more positive potential, $-0.5\ V_{SCE}$, is applied for 180 s. Both steps are repeated up to 30 times. As in case of constant potential deposition, the Fe-rich Fe–Pd alloy is deposited during the first step. The idea of the off-time during the second step is that no metal deposition at all should occur, allowing equalizing concentration gradients of metal ions as well as the ascension of hydrogen bubbles. The measured current during step 1 (inset Fig. 2e) reveals that the deposition is stopped before the cathodic current is decreased to the diffusion-limited region. This reduces the depletion of metal ions and blocking of pores. In the second step the current becomes temporary anodic, as expected for charge reversal of the double layer, but then reaches a small constant cathodic current (inset Fig. 2e). This might be attributed to a minor deposition a Pd-rich alloy. Fig. 2e illustrates the current–time characteristics over all cycles; the black squares highlight the end of each deposition step. The black curve shows a similar trend as for potentiostatic deposition: during the first cycles the final deposition current slightly decreases and becomes constant over around 10 cycles. When the final current starts to increase again the deposition was stopped. HR-SEM investigations confirm a clear improvement of nanowire quality (Fig. 2b) compared to constant deposition potentials (Fig. 2a). A more homogeneous filling and less fragmented nanowires of a length of approximately 1.5 μm and an integral composition of $Fe_{74}Pd_{26}$ (± 4 at.%) are achieved. Small dots or short wire like deposits above the wires top end and surface coverage are present.
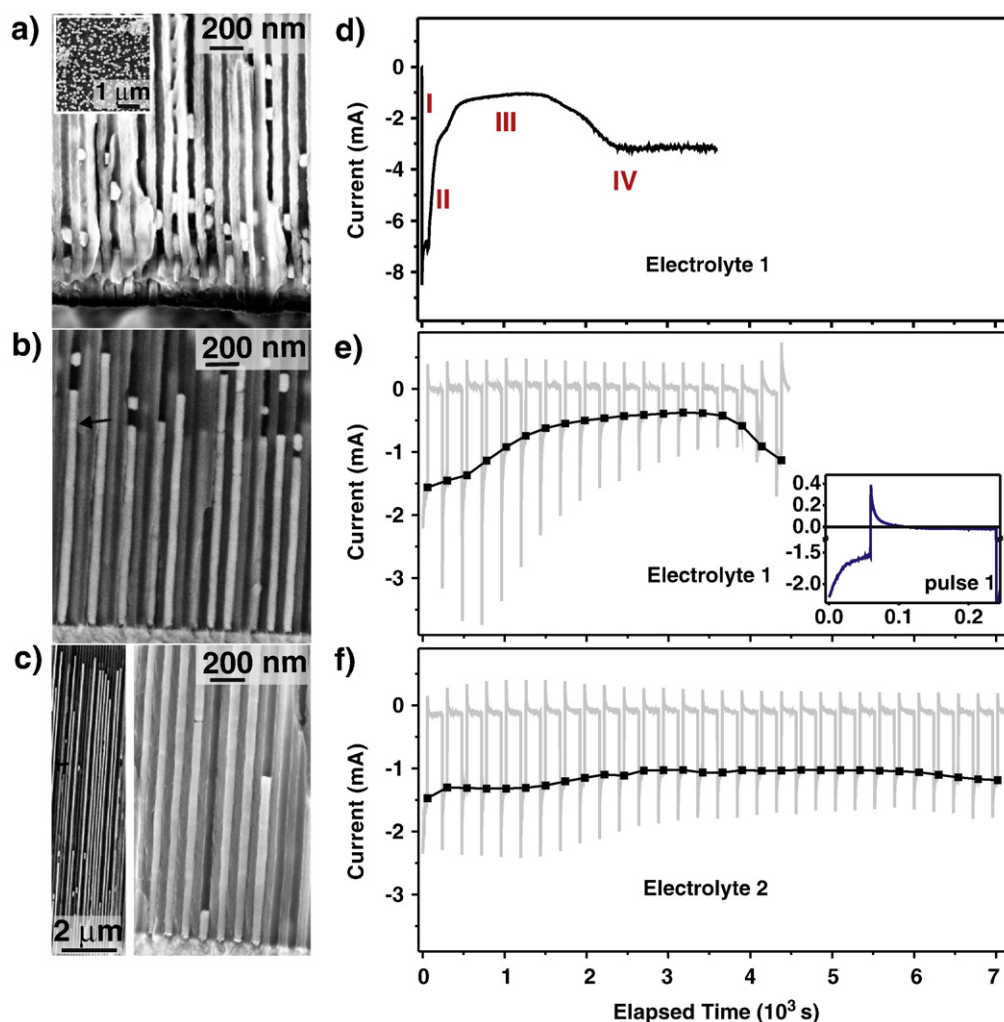
As alternating potentials could neither avoid short wire fragments nor surface coverage, there must be additional reasons for irregular filling in addition to pore blocking by hydrogen. Due to the strong difference in nobility an exchange reaction according to

$$Pd^{2+} + 2Fe^{2+} \rightarrow Pd + 2Fe^{3+} \tag{1}$$
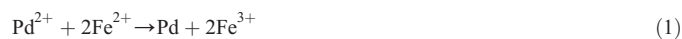
can easily occur electroless, resulting in the formation of Pd nuclei along pore walls and on the template surface. Once a Pd nucleus is formed FePd can be electrodeposited onto this nucleus additionally accounting for irregular non-uniform filling and explaining the higher Pd content of approximately 80 at.% at the surface.

Furthermore, this suggest that Eq. (1) is the reason for electrolyte instability. This instability is evident from the observed shiny film on the electrolyte surface and also after some hours of use from the coverage of vessels with a mirror like Pd surface.

In order to develop a stable FePd electrolyte Fe^{2+} is exchanged by Fe^{3+} (electrolyte 2). Thus the electroless formation of Pd nuclei according to Eq. (1) is inhibited. Accordingly, no more surface deposits had been

Fig. 1. Composition of Fe–Pd nanowires in alumina templates deposited from electrolyte 1 in dependence on the applied constant deposition potential.

Fig. 2. Cross-sectional HR-SEM micrographs Fe–Pd nanowires in alumina templates (left column) and associated current profiles (right column): deposited at a) and d) constant potentials from electrolyte 1; in pulsed potential mode from b) and e) electrolyte 1 and c) and f) electrolyte 2; ■ - marks the end of each deposition step; the inset in e) enlarges the 1st pulse.

observed on vessels or the sample surface. This proves the increased stability of the electrolyte. The measured current over deposition time (Fig. 2f) gives rise to optimized and more stable deposition conditions. As a main feature compared to the Fe^{2+} electrolyte the final cathodic current of each deposition step (marked with black squares) changes only slightly with cycle number, excluding any undesired or electroless deposition processes. Cross-sectional HR-SEM (Fig. 2c) reveals further improved nanowire morphology. Nanowire lengths up to 11 μm (Fig. 2c) with an integral composition of around $Fe_{68}Pd_{32}$ (± 2 at.%) have been reached. At highest resolution, indications of a material contrast along the wire axis become visible in the micrographs. Further TEM investigations will clarify if these originate from an inhomogeneous composition due to alternating potentials.

4. Conclusion

The successful preparation of Fe–Pd nanowires in alumina templates using a sulfosalicylic–ammonia-complexed electrolyte has been demonstrated. The utilization of $Fe_2(SO_4)_3 \cdot 9H_2O$ and an alternating potential procedure turned out to be the most effective combination. The use of trivalent instead of divalent iron ions and the approach of complexing both Fe^{3+} and Pd^{2+} ions stabilizes the electrolyte, brings their standard electrode potentials closer together and, therefore, makes a reproducible codeposition of Fe and Pd possible. After optimization of deposition conditions, nanowire arrays homogeneously filled with long and continuous wires close to the desired composition of $Fe_{70}Pd_{30}$ have

been obtained. No surface plating or deposits are observed. As within one template about 10^9 $Fe_{70}Pd_{30}$ nanowires can be prepared in one run, this approach represents a very efficient way towards magnetic shape memory nanowires for nanoactuation. A detailed study of the structural and magnetic properties will follow.

References

[1] K.J. Bryden, J.Y. Ying, Nanostruct. Mater. 9 (1–8) (1997) 485.
[2] S. Doi, F. Wang, K. Hosoiri, T. Watannabe, Mater. Trans., JIM 44 (2003) 649.
[3] R. Hultgren, C. Zapffe, Nature 142 (1938) 395.
[4] R.D. James, M. Wuttig, Philos. Mag. A 77 (5) (1998) 1273.
[5] T. Kakeshita, T. Fukuda, Mater. Sci. Forum 394–395 (2002) 531.
[6] C. Bechthold, J. Buschbeck, A. Lotnyk, B. Erkartal, S. Hamann, L. S. C. Zamponi, A. Ludwig, L. Kienle, S. Fähler, E. Quandt, Adv. Mat. (2010) in press, doi:10.1002/adma.201000599.
[7] S. Inoue, K. Inoue, K. Koterazawa, K. Mizuuchi, Mater. Sci. Eng. 339 (2003) 29.
[8] D. Vokoun, C.T. Hu, Scr. Mater. 47 (7) (2002) 453.
[9] J. Buschbeck, I. Lindemann, L. Schultz, S. Fähler, Phys. Rev. B: Condens. Matter 76 (20) (2007) 205421.
[10] F. Wang, S. Doi, K. Hosoiri, H. Yoshida, T. Kuzushima, M. Sasadaira, T. Watanabe, Electrochim. Acta 51 (2006) 4250.
[11] F.M. Takata, G. Pattanaik, W.A. Soffa, P.T. Sumodjo, G. Zangari, Electrochem. Commun. 10 (4) (2008) 568.
[12] D. AlMawlawi, N. Coombs, M. Moskovits, J. Appl. Phys. 70 (8) (1991) 4421.

[13] H. Zeng, M. Zheng, R. Skomski, D.J. Sellmyer, Y. Liu, L. Menon, S. Bandyopadhyay, J. Appl. Phys. 87 (9) (2000) 4718.

[14] K. Nielsch, F. Müller, A.P. Li, U. Gösele, Adv. Mat. 12 (8) (2000) 582.

[15] X. Fei, S. Tang, R. Wang, H. Su, Y. Du, Solid State Commun. 141 (1) (2007) 25.

[16] B.-Y. Yoo, S. Hernández, B. Koo, Y. Rheem, N. Myungk, Water Sci. Technol. 55 (2007) 149.

[17] H. Hu, C. Yang, J. Chen, G. Wu, J. Magn. Magn. Mater. 320 (18) (2008) 2305.

[18] H. Liu, F. Wang, Y. Zhao, J. Liu, K.C. Park, M. Endo, J. Electroanal. Chem. 633 (1) (2009) 15.

[19] S. Hernández, B. Yoo, E. Stefanescu, S. Khizroev, N. Myung, Electrochim. Acta 53 (18) (2008) 5621.

[20] P. Juzikis, M. Kittel, C. Raub, Plat. Surf. Finish. 81 (8) (1994) 59.

[21] M.E. Baumgärtner, D.R. Gabe, Trans. IMF 78 (2) (2000) 79.

[22] D. Landolt, Plat. Surf. Finish. 88 (9) (2001) 70.

[23] A.P. Li, F. Müller, A. Birner, K. Nielsch, U. Gösele, J. Appl. Phys. 84 (11) (1998) 6023.

[24] A. Kumar, S. Fähler, H. Schlörb, K. Leistner, L. Schultz, Phys. Rev. B 73 (6) (2006) 064421.

[25] V. Haehnel, S. Fähler, P. Schaaf, M. Miglierini, C. Mickel, L. Schultz, H. Schlörb, Acta Mater. 58 (7) (2010) 2330.